https://doi.org/10.5194/egusphere-2025-5424
Preprint. Discussion started: 27 January 2026

O_3–NO_x–VOC_s Sensitivity in Major Chinese Regions: Detailed Insights from GEMS Satellite Hourly Observations

Cheng Huang[1], Junjie Wang[1], Yinbao Jin[1,2], Min Min*[1], Qi Fan*[1,3,4],Jhoon Kim[5]
[1]School of Atmospheric Sciences, Sun Yat-sen University, Zhuhai, China
[2]Guangzhou Meteorological Satellite Ground Station (Guangdong Meteorological Satellite Remote Sensing Center), Guangzhou, China
[3]Southern Marine Science and Engineering Guangdong Laboratory, Zhuhai, China
[4]Guangdong Province Key Laboratory for Climate Change and Natural Disaster Studies, Sun Yat-sen University, Guangzhou, China
[5]Department of Atmospheric Sciences, Yonsei University, Seoul, South Korea

* *Correspondence*: Qi Fan(eesfq@mail.sysu.edu.cn) and Min Min(minm5@mail.sysu.edu.cn)

Abstract

Ozone (O_3) pollution continues to pose a severe environmental and public health challenge in China. Identifying whether ozone formation is more sensitive to nitrogen oxides (NOx) or volatile organic compounds (VOCs) is therefore fundamental to designing effective control strategies. This study investigates the diurnal evolution of O_3 formation sensitivity across major regions of China, utilizing high-temporal-resolution observations from the Geostationary Environment Monitoring Spectrometer (GEMS) from 2021 to 2023. By analyzing the formaldehyde-to-nitrogen dioxide ratio ($HCHO/NO_2$ or FNR) at an hourly scale (09:00–16:00 LST) during the warm season alongside ground-level O_3 measurements and meteorological reanalysis, we capture the dynamic daytime transitions in O_3–NOx–VOC chemistry. Results show distinct diurnal patterns: O_3 and HCHO concentrations generally increase through the afternoon, peaking around 15:00–16:00, while NO_2 declines with a morning rebound. Spatially, elevated precursor levels and complex sensitivity regimes are concentrated in key urban agglomerations (BTH, YRD, SC, PRD). The analysis reveals a systematic shift from VOC-limited regimes in the morning toward transitional or NOx-limited regimes in the afternoon, driven by intensified photochemistry. A comparative city-level analysis demonstrates that Beijing's strong radiation under NOx-rich conditions sustains a morning VOC-limited regime, Nanjing remains in a complex transitional state, Chengdu's basin topography reinforces a persistent VOC-limited condition, and Guangzhou's active VOC emissions promote a shift toward NOx limitation. This study provides the first regional-scale, diurnally-resolved insight into O_3 formation sensitivity dynamics in China, offering a critical scientific basis for designing temporally precise and regionally tailored emission control strategies.

1 Introduction

Near-surface ozone (O_3) pollution has emerged as a major environmental challenge in rapidly urbanizing countries such as China. Ozone is not only an important greenhouse gas that influences climate change (Akimoto, 2004), but also poses direct threats to regional air quality, public health, and ecosystems by altering atmospheric oxidizing capacity (Feng et al., 2022). Previous studies have shown that long-term exposure to O_3 has led to a substantial increase in premature mortality from respiratory and cardiovascular diseases in China (Maji and Namdeo, 2021), and has caused considerable yield losses in major crops such as rice and wheat (Feng et al., 2019). Ozone formation depends on complex

https://doi.org/10.5194/egusphere-2025-5424
Preprint. Discussion started: 27 January 2026

and nonlinear photochemical reactions between its precursors, nitrogen oxides (NO_x) and volatile organic compounds (VOC_s) (Sillman, 1995; Kleinman et al., 2005). Accordingly, ozone formation regimes are commonly classified into NO_x-limited, VOC-limited, and transitional regimes (Sillman and He, 2002). Therefore, accurately diagnosing the sensitivity of ozone formation to its precursors is a fundamental scientific prerequisite for the development of effective air pollution control strategies.

The column concentration ratio of formaldehyde to nitrogen dioxide ($HCHO/NO_2$, FNR) is one of the most widely used metrics for diagnosing ozone formation sensitivity (Chen et al., 2023; Wang et al., 2023). This indicator plays an important role in advancing the understanding of ozone formation mechanisms and in informing the design of region-specific air pollution control strategies (Jin et al., 2020). At present, FNR values are mainly derived from three types of data sources: instantaneous overpass observations from polar-orbiting satellites, chemical transport model simulations, or ground-based monitoring measurements. Numerous studies have employed FNR values calculated from these datasets to investigate their correspondence with ozone formation sensitivity, where higher FNR values generally indicate a NO_x-limited regime, whereas lower FNR values suggest a VOC-limited regime (Souri et al., 2020; Acdan et al., 2023). For example, in East Asia, Itahashi et al. (2022) reported an overall increasing trend in FNR values over Japan and South Korea based on Ozone Monitoring Instrument (OMI) satellite observations. In South Asia, Mahajan et al. (2015) compared observations from four different satellite instruments and found relatively high FNR values over India, implying that ozone formation is more likely to be NO_x-limited, while urban and industrialized regions exhibit distinct sensitivity characteristics. Jin et al. (2017) combined satellite observations with chemical transport modeling to reveal pronounced regional-scale differences in ozone formation sensitivity across major urban agglomerations in North America. For typical urban clusters in China, Zhou et al. (2024) reported, based on ground-based observations during April–September 2020, that urban Beijing was predominantly VOC-limited. Using OMI satellite data, Xu et al. (2025) found that ozone formation in the Sichuan–Chongqing (SC) region during summer was mainly characterized by a VOC–NO_x transitional regime, accounting for approximately 42.42% of the area. Pan (2023), integrating OMI satellite observations with ground-based measurements, demonstrated that northern parts of the Yangtze River Delta (YRD) had long been dominated by a transitional regime, with an areal fraction consistently around 50.0%, substantially higher than those of the VOC-limited and NO_x-limited regimes. Similarly, Liang et al. (2024), using OMI satellite data combined with grey relational analysis, reported that in 2020 the Pearl River Delta (PRD) exhibited areal fractions of 1.6%, 42.4%, and 56.0% for the VOC-limited, transitional, and NO_x-limited regimes, respectively; at the provincial scale of Guangdong, the NO_x-limited regime further increased to 86.4%. In contrast, Du et al. (2022b), employing the Comprehensive Air quality Model with extensions (CAMx), emphasized that the Chengdu metropolitan area was predominantly NO_x-limited and highlighted the critical role of industrial and mobile-source emission reductions in ozone mitigation. Collectively, these studies indicate that urban areas are more often characterized by VOC-limited or transitional regimes, whereas rural and background regions tend to be NO_x-limited, and that major urban agglomerations worldwide exhibit broadly similar patterns of regional differentiation in ozone formation sensitivity.

In addition to spatial heterogeneity, ozone formation sensitivity also exhibits pronounced temporal variability. Changes in meteorological conditions, surface characteristics, and anthropogenic emissions jointly drive transitions in ozone sensitivity across different time scales (Liu and Shi, 2021). On the interannual scale, the implementation of emission control policies has led to shifts in ozone sensitivity from VOC-limited regimes toward transitional or NO_x-limited regimes in many regions of China (Min

https://doi.org/10.5194/egusphere-2025-5424
Preprint. Discussion started: 27 January 2026

et al., 2021). At seasonal and monthly scales, ozone sensitivity also shows systematic variations; for example, under high-temperature and strong-radiation conditions in summer, NO_x-limited or transitional regimes are more prevalent, whereas VOC-limited regimes tend to dominate in spring and autumn (Li, 2023; Jing et al., 2025; Yang et al., 2025; Du et al., 2022a). Furthermore, studies based on observations and chemical transport modeling indicate that ozone sensitivity exhibits more complex behavior at the monthly scale, characterized by pronounced interconversions among different regimes. For example, Wu et al. (2018) found, through an analysis of ozone formation mechanisms in the Beijing–Tianjin–Hebei (BTH) region, that the area classified as VOC-limited increased markedly in September, while regions that were predominantly NO_x-limited during June–August gradually transitioned to a transitional regime in September, and portions of the transitional regime further shifted toward a VOC-limited regime. Xu et al. (2025) further pointed out that in the SC region, the fraction of VOC-limited areas gradually decreased from June to August, reaching a minimum in August with an areal proportion of only 4.02%. Similarly, Li (2021), based on numerical modeling and FNR threshold analysis, reported that in July most of the PRD region was characterized by a NO_x-limited regime, whereas by October, western Dongguan, western Shenzhen, the Nansha District of Guangzhou, and southeastern Foshan transitioned to a VOC-limited regime, with some areas further evolving into a transitional regime. These studies provide important support for a deeper understanding of ozone formation mechanisms. However, a key question that remains insufficiently addressed is whether ozone formation sensitivity—given the pronounced diurnal variability of ozone—also undergoes systematic and regular transitions on the diurnal timescale.

A key challenge is that the three prevailing approaches mentioned above for calculating FNR all have inherent limitations in investigating diurnal variability. (1) Polar-orbiting satellite products (such as OMI and TROPOspheric Monitoring Instrument (TROPOMI)) provide only a single overpass "instantaneous snapshot" per day, which is insufficient to capture the continuous diurnal evolution of ozone formation sensitivity (Lyu et al., 2024; Bhartia et al., 2002; Grytsai and Milinevsky, 2013; Zhang et al., 2018; Peng et al., 2024). In addition, these observations are highly susceptible to cloud contamination, leading to data gaps and spatial discontinuities that can introduce biases in satellite-derived products (Li and Chen, 2021). (2) Numerical models can deliver hourly data products, but their results depend strongly on the accuracy of meteorological inputs, emission inventories, and chemical mechanisms. Even the most recent chemical mechanisms (such as Mechanism for Atmospheric Chemistry eXtended 1 (MAX1)) are still being continuously refined to improve simulation performance (Liu et al., 2025; Pan, 2023; Chen et al., 2022; Wang et al., 2022). Moreover, uncertainties associated with meteorological forcing, emission magnitudes and temporal allocation, chemical reactions among pollutants and deposition processes can further propagate substantial uncertainties in model results (Georgiana et al., 2016; Yu et al., 2020). (3) Ground-based observations offer high temporal resolution but suffer from sparse and uneven station coverage, resulting in limited spatial representativeness and an inability to depict complete regional-scale diurnal patterns (Yang et al., 2013; Xu et al., 2024; Klára et al., 2019; Wang et al., 2025b; Bin et al., 2022; Zhang et al., 2020; Han et al., 2023). For individual sites, ozone research relies primarily on longitudinal time-series analyses, in which comparisons with satellite observations are used to validate data accuracy or to identify temporal patterns for assessing long-term trends in local ozone levels. Indeed, Wang et al. (2019), when analyzing the spatiotemporal variability of surface ozone column concentrations in China using data from six stations, also highlighted these limitations and emphasized the need for broader spatial coverage to robustly evaluate ozone. Consequently, none of these three mainstream approaches can

https://doi.org/10.5194/egusphere-2025-5424
Preprint. Discussion started: 27 January 2026

simultaneously provide high temporal resolution and extensive spatial coverage to directly and reliably characterize the true diurnal evolution and spatial patterns of O_3 formation sensitivity.

This study leverages observations from the Geostationary Environment Monitoring Spectrometer (GEMS) to fill the knowledge gap regarding the diurnal dynamics of ozone formation sensitivity. Unlike the "instantaneous snapshots" provided by polar-orbiting satellites, GEMS enables continuous "staring" observations over Asia, thereby allowing, for the first time, the investigation of the FNR at an hourly resolution on a regional scale. Building on this capability, we systematically examine the hourly spatiotemporal evolution of FNR across China from morning to afternoon, with the aim of elucidating the diurnal transitions in ozone formation mechanisms and identifying their driving factors.Specifically, this study addresses two key questions: (1) What spatiotemporal patterns characterize the diurnal evolution of ozone formation sensitivity (FNR) across different regions of China during daytime (09:00–16:00 LST)? (2) Do these diurnal transition patterns differ among major urban agglomerations in China, and what are the dominant factors driving these differences? The findings of this work enable the identification of ozone-sensitive periods and key regions with unprecedented spatiotemporal detail, providing direct scientific support for the implementation of dynamic, time-resolved, region-specific, and category-based emission reduction strategies. More importantly, they contribute to a fundamental understanding of the diurnal dynamics of nonlinear photochemical processes governing ozone formation, facilitating a paradigm shift in regional air quality management from "static control" toward "dynamic regulation". This study provides crucial insights into the temporal dynamics of O_3 pollution, offering a scientific basis for its coordinated management in China.

2 Data and Methods

2.1 Dataset

To enhance air quality monitoring and climate change forecasting in East and Southeast Asia, the National Institute of Environmental Research (NIER) of South Korea developed the new-generation and first GEMS aboard the Geostationary (GEO) Korea Multi-Purpose Satellite 2B (GEO-KOMPSAT-2B). This satellite was successfully launched in February 2020. GEMS operates at a spectral resolution of 0.6 nm, covering a wavelength interval of 0.2 nm across the 300-500 nm range (Kim et al., 2020). It provides hourly observations across Asia, from 5°S to 45°N and 75°E to 145°E, with a spatial resolution of 7 × 8 km. This instrument primarily tracks key atmospheric components, including NO_2, O_3, HCHO, and aerosols. GEMS offers significant advantages over other satellites with its exceptional temporal resolution, collecting data eight times daily (00:45 to 07:45 UTC) (Kim et al., 2020; Baek et al., 2023). As depicted in Fig. 1, GEMS covers most of China from 08:45 LST to 15:45 LST with an interval of 1 hour. LST was used for all study times in this paper if not otherwise stated. The study area for GEMS eight observation periods is defined as 17-43°N, 97-127°E, with a spatial resolution of 0.07° × 0.08°. Additionally, the observation window has been adjusted to 09:00 to 16:00, crucial for monitoring photochemical activities and urban emissions in major Chinese cities (BTH, YRD, PRD, SC, in Fig.1c. GEMS level-2 tropospheric NO_2 and HCHO data from 2021 to 2023 are free to download at https://nesc.nier.go.kr/ko/html/index.do. It has also demonstrated high correlation coefficients (R) of 0.9 with the NO_2 data of TROPOMI and 0.81 with ground-based HCHO observations, affirming its reliability and effectiveness in capturing accurate atmospheric data (Lee et al., 2024; Kim and Kim, 2023; Oak et al., 2024).

https://doi.org/10.5194/egusphere-2025-5424
Preprint. Discussion started: 27 January 2026

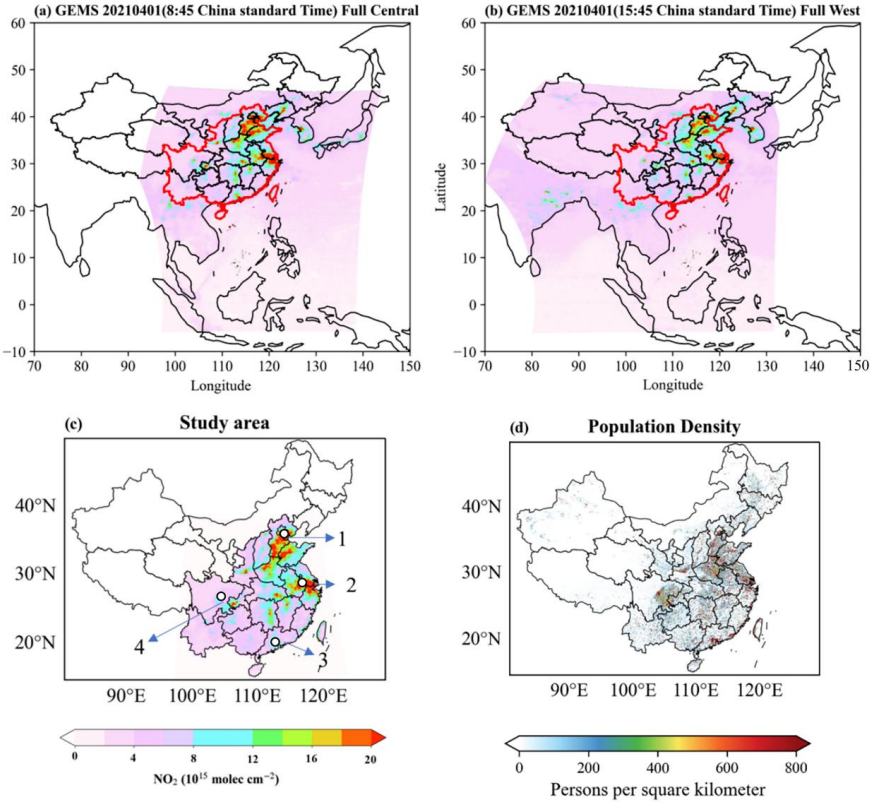

Figure 1. (a) NO_2 in the Full Central (FC) region as inverted by GEMS satellite at 8:45 LST on April 1, 2021. **(b)** NO_2 in the Full West (FW) region as inverted by GEMS satellite at 15:45 LST on April 1, 2021, and (c) the study area of this study (the red combined region in panel (a)), where regions 1 – 4 denote the BTH, YRD, PRD, and SC regions, respectively. The white circular symbols from north to south indicate Beijing, Nanjing, Chengdu, and Guangzhou. (d) Spatial distribution of population density in China, 2017, the population data for the study area**((a)** red ensemble area**)** represents approximately 87% of the country's total population.

The China National Air Quality Monitoring Network provides hourly surface O_3 measurements through an extensive network of over 1,400 ground-based stations in more than 330 cities across China. This invaluable data can be accessible through the official website at https://air.cnemc.cn:18007/. Our analysis includes data from 642 stations located in 210 cities, with all O_3 concentrations recorded in micrograms per cubic meter (μg/m³). Many scholars have studied Ozone-NO_x-VOC_s sensitivity using satellite-observed tropospheric NO_2 and HCHO concentrations along with near-surface O_3 data, and therefore the above GEMS data and site data were selected for this study (Jin et al., 2020; Ren et al., 2022). Additionally, this study incorporates hourly ERA5 reanalysis data, provided by the European Centre for Medium-Range Weather Forecasts (ECMWF). The ERA5 dataset includes critical meteorological variables such as 2-meter temperature (T_{2m}), relative humidity (RH), near-surface net radiation flux (SSR), and boundary layer height (BLH). These variables provide comprehensive insights into the meteorological conditions affecting ozone formation and its diurnal variations across the study area, enhancing the understanding of O_3-NO_x-VOC_s interactions.

https://doi.org/10.5194/egusphere-2025-5424
Preprint. Discussion started: 27 January 2026

2.2 Methodology

The Locally Estimated Scatterplot Smoothing (LOESS) method is a non-parametric regression technique used to capture the underlying patterns in data, particularly useful for modeling complex relationships. It works by fitting simple models (usually linear or quadratic) to localized subsets of the data, rather than the entire dataset at once. This approach helps to smooth out fluctuations and reveal trends by applying different weights to data points based on their distance from a target point. In this study, LOESS was employed to analyze the diurnal variations of the HCHO/NO_2 ratio, which serves as an indicator of O_3 formation sensitivity. By focusing on hourly shifts in this ratio, the method effectively highlights local trends and transitions in the O_3-NO_x-VOC_s sensitivity regimes throughout the day. Its ability to reveal intricate patterns makes LOESS particularly valuable in examining ozone formation processes, which are known to exhibit non-linear dynamics and significant spatiotemporal variability. This adaptive smoothing approach thus provides a clearer understanding of diurnal changes in O_3 precursors and their interactions, contributing to more accurate interpretations of GEMS satellite observations.

3 Results and Discussion

3.1 Spatial distribution of HCHO, NO_2, and O_3

Figure. 2 based on GEMS data and ground monitoring, shows daily variations in atmospheric pollutants in China during the warm season (April to September) from 2021 to 2023, including the tropospheric column concentration of HCHO and NO_2, as well as the ground-level concentrations of O_3. At 09:00, higher initial concentrations of HCHO relative to NO_2 are apparent, likely from reduced nighttime dispersion and increased morning emissions (Yang et al., 2017). The majority of HCHO is produced through photo-oxidation of VOC_s, while relatively little is emitted directly (Sun et al., 2021). As the day progresses, increases in temperature and radiation intensity promote the conversion of VOC_s to HCHO (Eq. 1), significantly increasing HCHO levels, especially in densely populated urban areas (Fig. 1) with larger concentrations of VOC_s such as BTH, YRD, PRD, and SC. Wu et al. (2023) demonstrated that HCHO concentration increased with increasing photochemical activity, especially in the afternoon when solar radiation is strongest. The HCHO peaks around 16:00, correlating with findings by Lee et al. (2024). Although the reaction of HCHO with OH radicals serves as a consumption mechanism (Eq. 2), in regions with high VOC emissions, the continuous conversion of both biogenic and anthropogenic VOC_s, driven by increasing temperature and radiation, may result in a net production rate of HCHO that surpasses its consumption rate, thereby leading to a sustained increase in HCHO concentrations during the afternoon period (Li et al., 2021; Javed et al., 2019). HCHO increases steadily for the day, reaching approximately 1.3 times the 9:00 level by 16:00. Simultaneously, NO_2 levels show significant diurnal fluctuations, with high morning levels from traffic and industrial activities and minimal photochemical reduction due to low solar intensity (Fig. 3) (Xie et al., 2016). As sunlight and temperatures rise, intensified photochemical activities facilitate NO_2 consumption (Eqs. 3 and 4), leading to a gradual decline in its levels throughout the day. The most rapid reduction of NO_2 during the 13:00-14:00 hours is mainly due to rapid photochemical transformations and a strong diffusion effect due to the highest boundary layer height (Fig. 3). However, after 16:00, as photochemical activity diminishes and traffic increases in some cities due to school dismissals and varying work shifts, NO_2 levels rise again (Zhang and Batterman, 2009; Kelly et al., 1984). This trend is consistent with observations by Kim et al. (2020) and Elise and Tracey (2020). NO_2 peak in the morning and then gradually decline, reaching around 70% of their initial level by

https://doi.org/10.5194/egusphere-2025-5424
Preprint. Discussion started: 27 January 2026

15:00, followed by a slight rebound in the late afternoon. Although NO_2 is also regenerated during this process (Eqs. 5-7), increased photolytic activity and the conversion of NO_2 to nitric acid (Eq. 8) typically decrease NO_2 concentrations throughout the daytime (Tan et al., 2019). The peak of O_3 occurs between 15:00 and 16:00, with concentrations gradually increasing throughout the day, starting from a morning average of 56.29 $\mu g/m^3$ and reaching a peak of 122.32 $\mu g/m^3$ around 15:00. Liu and Wang (2020) and Xia et al. (2021) also reported that high O_3 concentrations during the warm season peak around 15:00 in major city clusters in China. Overall, the spatial distribution of HCHO, NO_2, and O_3 concentrations reveals significant regional differences across China. In the morning, high concentrations of HCHO and NO_2 are primarily concentrated in urban clusters, reflecting the impact of industrial activities and traffic emissions on the precursors of O_3. Meanwhile, O_3 concentrations are predominantly concentrated in the northern regions. In the afternoon, both HCHO and ozone concentrations increase significantly, with their distribution range notably expanding compared to the morning, particularly in high-population-density urban areas. However, high concentrations of NO_2 remain primarily concentrated in northern China, but due to the influence of local meteorological conditions, industrial emissions, and the involvement in O_3 formation, NO_2 concentrations gradually decrease.

$$VOC+OH \rightarrow RO_2+ \text{other by-products (e.g., HCHO)} \quad (1)$$

$$HCHO+OH+ O_2 \rightarrow H_2O+HO_2+CO \quad (2)$$

$$NO_2 + h\nu\ (UV) \rightarrow NO + O \quad (3)$$

$$O + O_2 + M \rightarrow O_3 + M \quad (4)$$

$$O_3+NO \rightarrow NO_2 + O_2 \quad (5)$$

$$RO_2+NO \rightarrow NO_2+RO \quad (6)$$

$$HO_2+NO \rightarrow NO_2+OH \quad (7)$$

$$NO_2+OH+M \rightarrow HNO_3+M \quad (8)$$

$$HCHO+h\nu\ (UV) \rightarrow 2HO_2+CO \quad (9)$$

Here, VOC_s react with hydroxyl radicals (OH), producing peroxy radicals (RO_2) and by-products like HCHO. RO_2 and HCHO can further react with nitrogen monoxide (NO), forming NO_2. NO_2 undergoes photolysis ($h\nu$), breaking down into NO and atomic oxygen (O), which combines with molecular oxygen (O_2) to form O_3. O_3 can react with NO to regenerate NO_2, maintaining the NO_x (NO + NO_2) cycle. Meanwhile, HCHO can photolyze into carbon monoxide (CO) and more hydroperoxyl radicals (HO_2), accelerating O_3 formation. NO_2 can also react with OH and a third body (M) to form nitric acid (HNO_3), reducing NO_x levels and limiting further O_3 production.

https://doi.org/10.5194/egusphere-2025-5424
Preprint. Discussion started: 27 January 2026

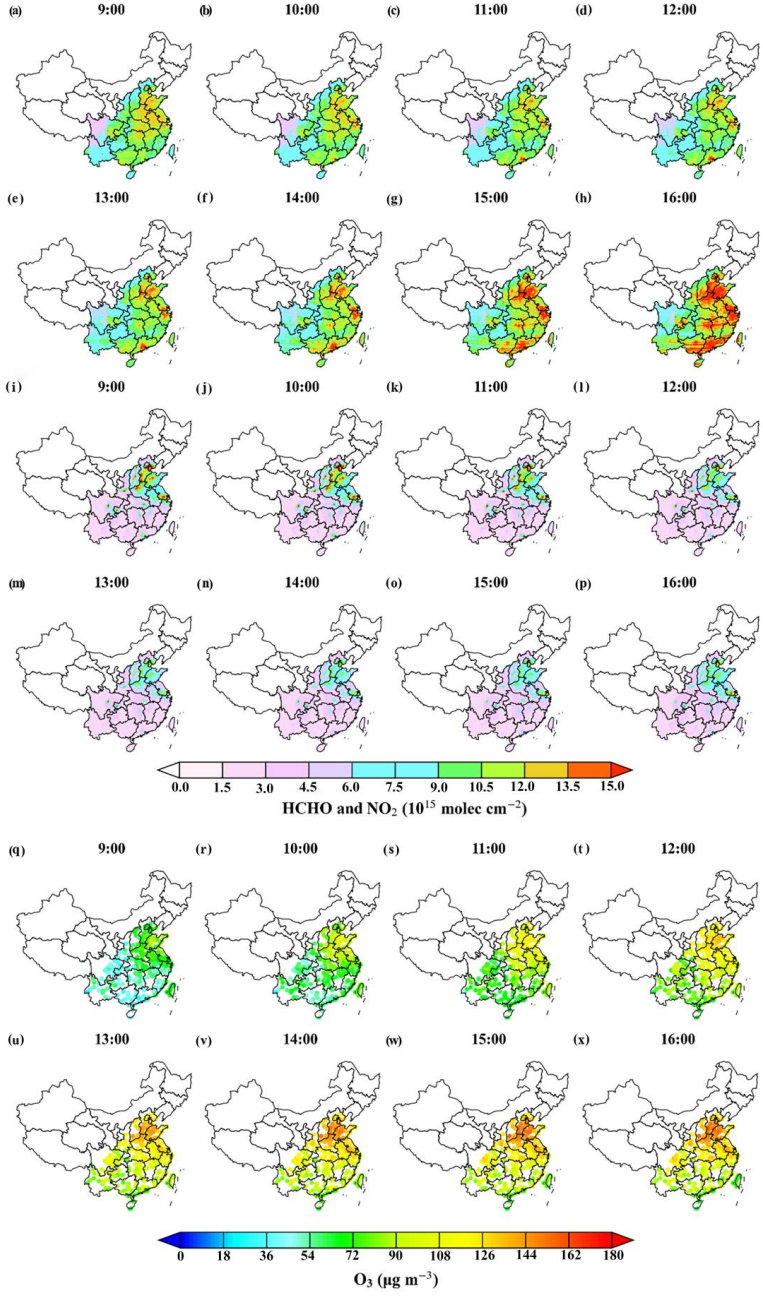

Figure 2. Hourly atmospheric monitoring in China during the warm season (April to September 2021-2023). **(a-h)** and **(i-p)** Spatial distribution of hourly mean HCHO and NO_2 levels retrieved from GEMS satellite data. **(q-x)** Temporal variations in ground-level mean O_3 concentrations, observed at various monitoring stations.

https://doi.org/10.5194/egusphere-2025-5424
Preprint. Discussion started: 27 January 2026

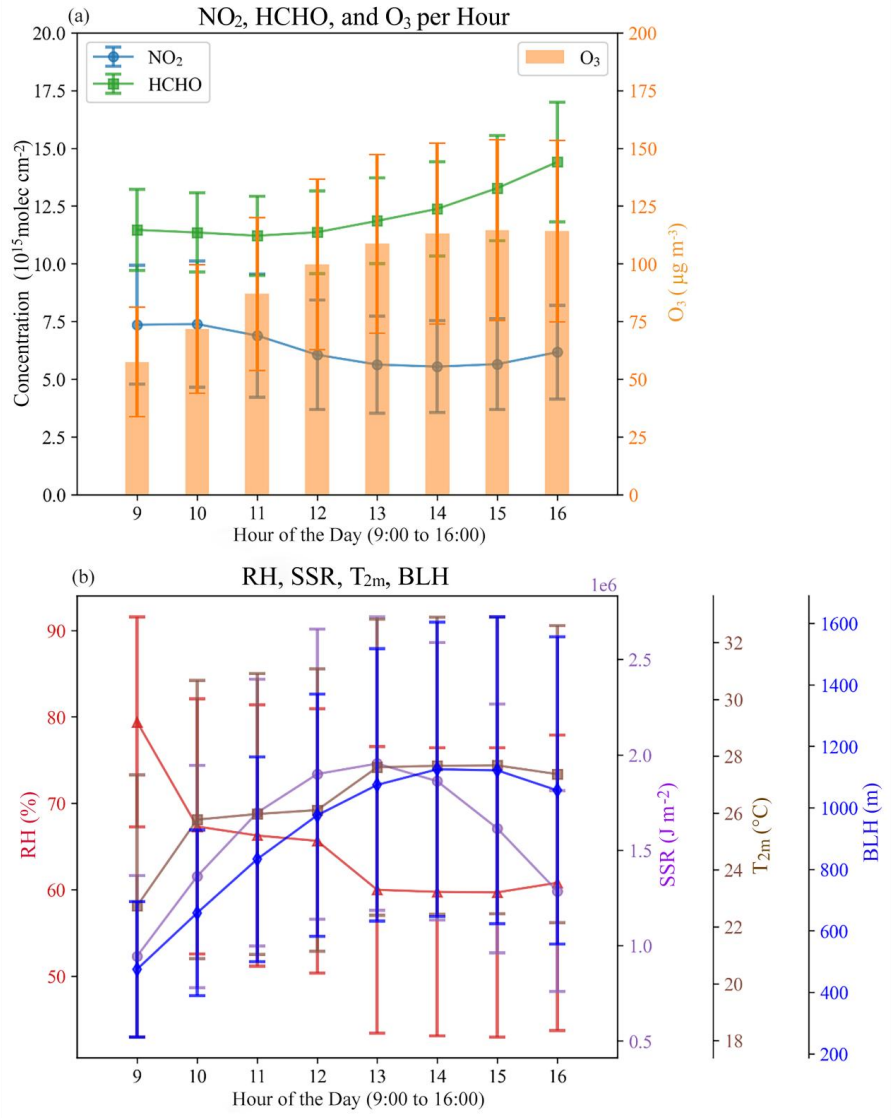

Figure 3. (a) Warm-season hourly ozone averages and deviations for all stations in the study area, with corresponding HCHO and NO_2 from GEMS. **(b)** and ERA5 corresponding to T_{2m}, RH, SSR, and BLH at the closest point site.

3.2 O_3–NO_x–VOC_s chemistry captured by GEMS satellite-based HCHO/NO_2

Figure. 4 displays the daily relationship between HCHO and NO_2 concentrations and ground-level O_3 utilizing LOESS fitting method to highlight trends and high O_3 concentration events. The distributions of HCHO and NO_2 at 09:00 are dispersed. The concentration of O_3 is relatively low in Fig. 4a, so the photochemical reaction required for O_3 formation has not yet started completely because of the low temperature and radiation (Fig. 3). At this time, data points ($NO_2 > 20 \times 10^{15}$ molec $\cdot$ cm^{-2}) are concentrated in the upper left corner, suggesting a NO_x-saturated state with VOC_s (represented by HCHO) as the limiting factor. In addition, a small amount of O_3 reacts with NO to form new NO_2 at

https://doi.org/10.5194/egusphere-2025-5424
Preprint. Discussion started: 27 January 2026

this time (Eq. 5), but its contribution is smaller than the impact of direct emissions and the effect of nighttime accumulation (Paul et al., 2018). From 10:00 to 12:00, as sunlight and temperature rise, data points move towards the lower right, significantly increasing O_3 concentration. During this period, three typical states of O_3-NO_x-VOC_s chemical processes can be identified: the VOC-limited regime, the transition zone, and the NO_x-limited regime. In the afternoon, data are mostly in areas of high HCHO and low NO_2, efficient O_3 production in HCHO-rich environments, even with low NO_2, resulting in the day's highest O_3 levels. The photochemical reaction of VOC_s is accelerated with increasing solar radiation (peak at 13:00) and temperature, generating more free radicals and intermediates (e.g., HCHO). The increase of these free radicals will further promote the photolysis of NO_2 and accelerate the generation of O_3. At the same time, the photolysis of NO_2 not only produces O_3 directly but also reduces the concentration of NO_2, reducing the O_3 consumption reaction (Yang et al., 2021). In addition, the lower relative humidity reduces the involvement of water vapor, which usually consumes O_3, and this reduction favors the accumulation of O_3 (Zhang et al., 2022). Since the reaction of VOC_s and NO_2 photolysis are mutually reinforcing, O_3 production in this environment shows a nonlinear enhancement, which is particularly evident under conditions of abundant VOC_s but low NO_2. Although there are some differences in the concentration and spatial distribution of HCHO and NO_2 between the GEMS and TROPOMI satellite data (Fig. 5), they all exhibit similar distribution characteristics of high values in the four major urban agglomerations (BTH, YRD, SC, and PRD). Specifically, the areas of high concentrations of HCHO and NO_2 are the same in both data, while the HCHO/NO_2 ratio also exhibits a similar spatial pattern. This similarity is further verified by the difference values (Fig. 5i), which show that the difference between the two ratios in major urban agglomeration regions is relatively small, indicating that both GEMS and TROPOMI data are effective in capturing the nonlinear relationship of precursors in the O_3 formation mechanism.

After establishing these nonlinear relationships across most of China, we further explored the diurnal variation characteristics of the quantitative relationship between high O_3 event probabilities and FNR observed by GEMS satellites, as shown in Fig. 4(i-p). Compared to cubic polynomial fitting (Fig. 6), we found that LOESS fitting performed better in identifying peak probabilities of high O_3 events with minimal uncertainty. During the morning hours (from 09:00 to 12:00), O_3 concentrations gradually increase within the transition ranges of [0.94, 1.46] to [1.36, 2.07], with fitting curves that are steep and closely aligned to the y-axis, indicating a rapid shift from a VOC-limited to a regime significantly influenced by HCHO and NO_2. As solar radiation intensifies and emissions from traffic and industrial sources continue, O_3 gradually accumulates near the ground. Note that the maximum FNR position gradually shifts rightward, indicating the growing importance of NO_2 in O_3 formation. In the afternoon (after 12:00), the fitted regimes, with broader transition zones spanning [1.30, 2.22] to [1.36, 2.28], more accurately captured the nonlinear relationship of O_3-NO_x-VOC_s ($R^2 > 0.88$) than those in the morning. The afternoon typically meets peak radiation and temperatures (Fig. 3), accelerating chemical reactions, especially photochemical reactions, thus enhancing O_3 production (Coates et al., 2016). Besides, the stable emissions and atmospheric chemical processes lead to consistent O_3 sensitivity curves from 13:00 to 16:00. Throughout the day, the maximum high-probability O_3 values from GEMS LOESS fitting increase, peaking at 1.97 at 15:00, before declining at 16:00. The O_3 sensitivity thresholds at 13:00 in this study align with previous findings, such as [1.0, 2.0] by Jin and Holloway (2015), and [1.5, 2.3] by Chang et al. (2016). Furthermore, GEMS data further revealed that the hourly variability in O_3-NO_x-VOC_s sensitivity throughout the day was more complex and dynamic compared to previous studies, which primarily reported diurnal

https://doi.org/10.5194/egusphere-2025-5424
Preprint. Discussion started: 27 January 2026

changes limited to a single time period, as observed by polar-orbiting satellites.

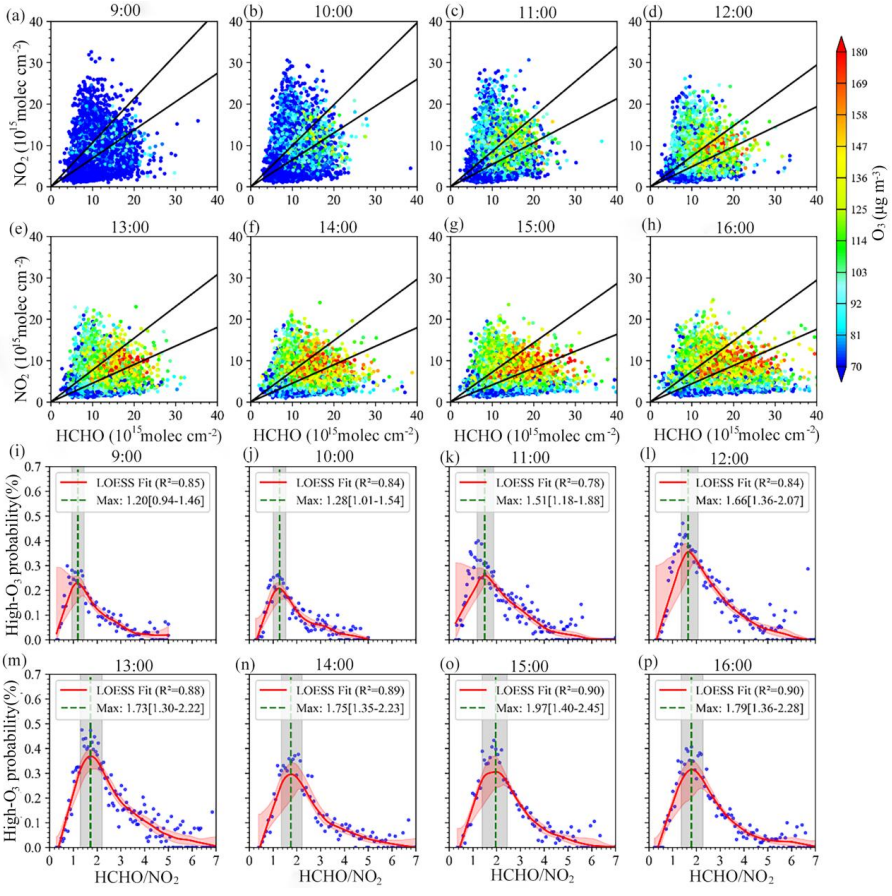

Figure 4. The relationship between hourly surface O_3 levels and GEMS HCHO/NO_2 from 2021 to 2023, analyzed using LOESS. **(a-h)** O_3 concentrations versus GEMS HCHO and NO_2. All surface hourly O_3 observations (9:00-16:00 LST) during the warm season from 2021 to 2023 were aggregated according to the corresponding GEMS HCHO and NO_2. The black line represents the hourly LOESS fit FNR values for GEMS data. **(i-p)** show the relationship of HCHO/NO_2 (x-axis) to high O_3 probability (y-axis), with data organized into 200 bins. Each bin represents a half-monthly average matched with corresponding hourly O_3 levels. Defined high O_3 event thresholds: 9:00 > 80 μg/m³, 10:00 > 100 μg/m³, 11:00 > 110 μg/m³, 12:00 > 120 μg/m³, 13:00 > 130 μg/m³, 14:00 and later > 140 μg/m³. The red line indicates the LOESS fit, with shading showing the 95% confidence interval. Bootstrap analysis with 1000 iterations was performed to ensure robustness, with each iteration involving random sampling and LOESS fitting. A vertical line and shading mark the peak and initial 15% transition range of the fitted curve, respectively.

https://doi.org/10.5194/egusphere-2025-5424
Preprint. Discussion started: 27 January 2026

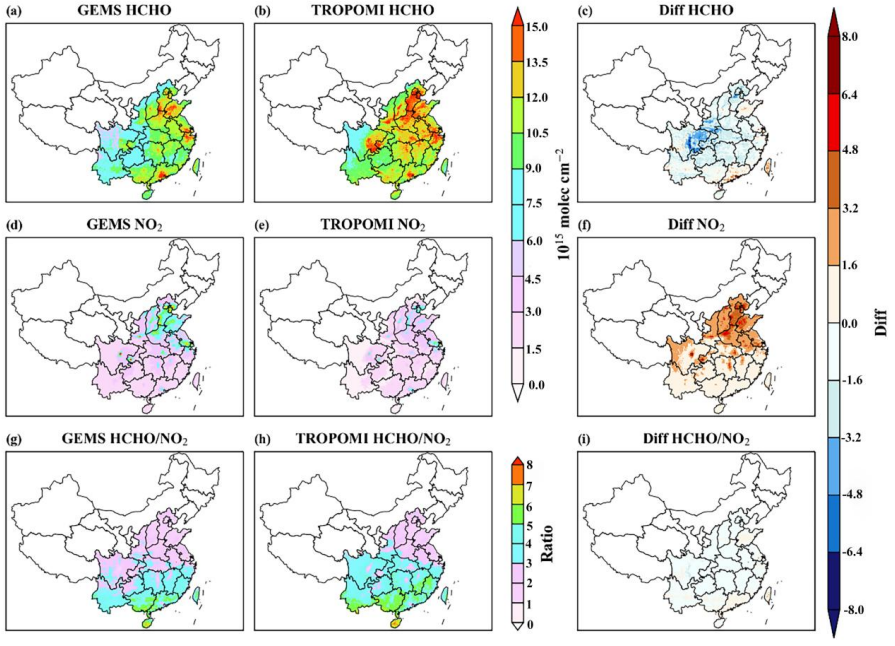

Figure 5. Mean values of HCHO, NO_2, and HCHO/NO_2 at 13 p.m. LST from 2021 to 2023 retrieved from GEMS and TROPOMI satellite data and their respective differences.

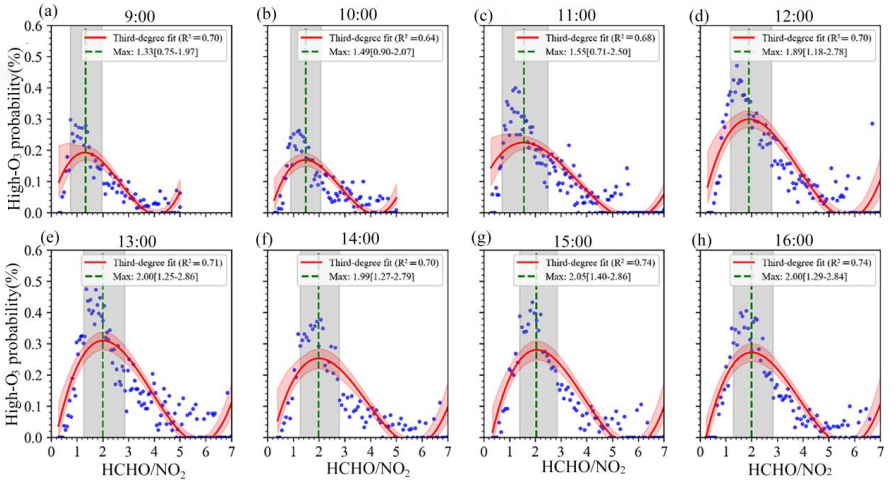

Figure 6. Similar to **Figure 4(i-p),** but with a third-order polynomial fit.

3.3 Spatiotemporal distribution of O_3 production regimes

In the afternoon (from 13:00), many urban areas initially VOC-limited in the morning start shifting to transition regimes (Fig. 7). The photochemical reactions of VOC_s are accelerated with increasing sunlight (peaking in the late afternoon), temperature (Fig. 3) and these reactions produce more free radicals and intermediates (Eqs. 1 and 9), such as HCHO. In addition, NO_2 is also rapidly photolyzed to NO and O (Eq.3), which not only contributes directly to O_3 production but also leads to a

https://doi.org/10.5194/egusphere-2025-5424
Preprint. Discussion started: 27 January 2026

further reduction in NO_2 concentration. Altogether, these conditions may accelerate the transition from VOC-limited to a state influenced by both NO_x and VOC_s (transition regimes) in many urban areas. Specifically at 13:00, VOC-limited regimes are primarily concentrated in downtown areas, aligning with former findings from TROPOMI-based studies (Li et al., 2024; Ren et al., 2022). However, the regimes are less extensive. In specific city clusters, apart from the PRD, the other three primarily maintain VOC-limited regimes in the morning but begin transitioning by the afternoon. It is worth noting that the PRD region exhibits specific photochemical changes throughout the day, with transition regimes in the morning and NO_x-limited regimes in the afternoon. The higher temperature and humidity conditions in the PRD may accelerate the reactions of VOC_s and NO_x, thereby affecting the formation of O_3. This hypothesis aligns with the findings of Wang et al. (2024) regarding the photochemical reaction rates in the PRD. In addition, air quality policies in the PRD in recent years have significantly reduced the concentrations of VOC_s and NO_x, which may contribute to the region's shift from a VOC-limited to a NO_x-limited regime (Li et al., 2024). Combined with Fig. 8 (same as Fig.7, but for 2021 and 2022), it is also evident that the PRD has recently begun transitioning from VOC-limited to NO_x-limited and transitional regimes in the morning. In addition, most urban centers are VOC-limited in the morning and start transitioning to NO_x-limited at the urban edge by the afternoon. Futhermore, the geographical characteristics of the SC may contribute to limited atmospheric circulation, fostering the formation of a pronounced temperature inversion layer. This phenomenon partially inhibits the dispersion of air pollutants, resulting in the region predominantly experiencing a VOC-limited regime during the daytime (Yang et al., 2020). Notably, the intensity of the VOC-limited regimes in the SC diminishes in the afternoon and is not particularly strong in the morning, likely influenced by the solar intensity and its effects on atmospheric dynamics.

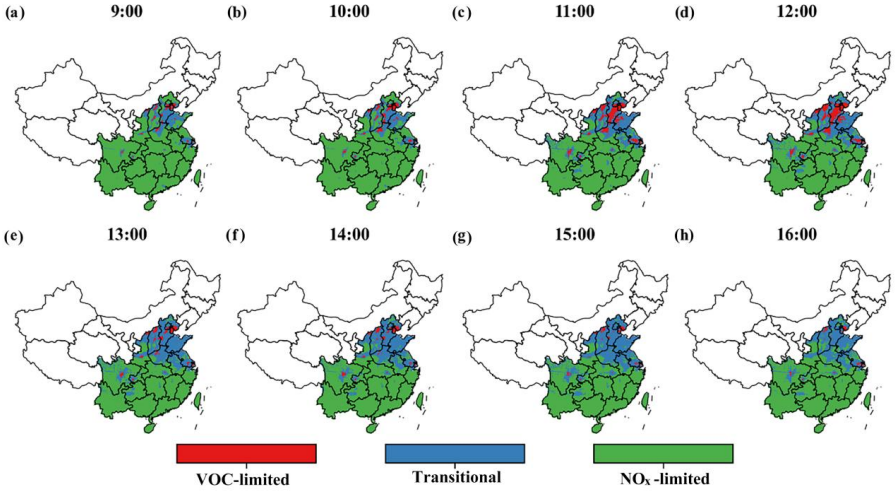

Figure 7. Diurnal photochemical-regime classification over study areas in O_3 pollution period from April to September 2023. **(a-h)** the analysis utilizes eight-hourly $HCHO/NO_2$ ratio data from the GEMS satellite to classify the regional O_3 formation dynamics in polluted areas (regions with GEMS NO_2 columns exceeding 1.0×10^{15} molec•cm^{-2}), The classification thresholds for VOC-limited, transitional, and NO_x-limited conditions are based on the relationship between hourly surface high O_3 occurrence probabilities and GEMS $HCHO/NO_2$,

https://doi.org/10.5194/egusphere-2025-5424
Preprint. Discussion started: 27 January 2026

as shown in **Figure. 4**.

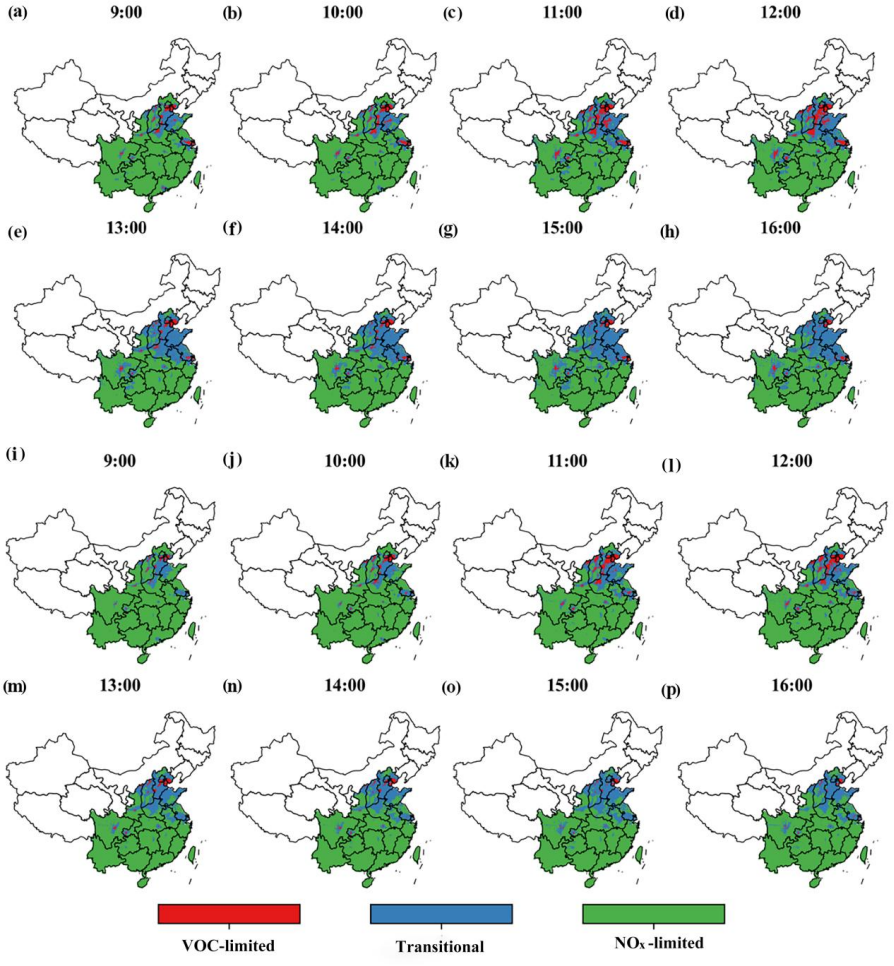

Figure 8. Similar to **Figure 7**, but for 2021 **(a-h)** and 2022 **(i-p)**.

3.4 Analysis of O_3 Formation Mechanisms in Representative Cities

Four representative cities — Beijing, Nanjing, Chengdu, and Guangzhou — were selected to represent the BTH, YRD, SC and PRD regions, respectively. As shown in Fig. 9(a-d), except for Guangzhou, the other three cities exhibit a high proportion of VOC-limited regimes during daytime. Notely, the VOC-limited fraction in Beijing and Chengdu peaks around noon (12:00). The changes in ΔHCHO and ΔNO_2, along with their rate-of-change ratio ($|\Delta HCHO/\Delta NO_2|$), serve as a robust indicator for tracking the dynamic response of relative precursor conversion intensities. With this analytical framework, we integrate hourly meteorological conditions (Fig. 9(e–h)) with the rates of change in ΔHCHO and ΔNO_2 (Fig. 9(i–l)) to conduct a comparative analysis of ozone formation mechanisms and their diurnal evolution.

Beijing is characterized by the coexistence of VOC-limited and transitional regimes between

https://doi.org/10.5194/egusphere-2025-5424
Preprint. Discussion started: 27 January 2026

09:00 and 16:00, reflecting a NO_2-abundant environmen. More specifically, Beijing remains predominantly VOC-limited from 09:00 to 13:00, after which the fractions of the NO_x-limited and transitional regimes gradually increase. Notably, taking 12:00 as a turning point, the VOC-limited fraction increases hourly before noon while the other regimes decrease, whereas after 12:00 the VOC-limited fraction declines sharply and reaches a minimum at 16:00, accompanied by a concurrent increase in the other two regimes, which peak at the same time. Strong SSR, particularly between 12:00 and 13:00, together with a rapidly increasing BLH, substantially enhances NO_2 photolysis and weakens the titration of O_3 by NO. As a result, even under high-NO_x emission conditions, ozone formation is unlikely to enter a NO_x-limited regime and is instead more strongly constrained by VOC_s availability. Previous studies have shown that under NO_x-rich conditions, ozone production is more sensitive to VOC_s, and that boundary layer development and enhanced radiation further amplify this sensitivity (Ren et al., 2022; Wang et al., 2025a). Consistently, Fig. 9i shows a relatively large net loss rate of NO_2, whereas the increase in HCHO is comparatively limited, leading to low values of $\Delta HCHO/\Delta NO_2$ in the morning and further indicating VOC-limited ozone formation under a NO_x-abundant background. In the afternoon, $\Delta HCHO/\Delta NO_2$ begins to increase, suggesting a transition toward a transitional regime with emerging NO_x-limited characteristics.

O_3 formation in Nanjing exhibits a more complex diurnal evolution, characterized by a predominantly transitional regime jointly controlled by VOC_s and NO_x, alongside a non-negligible contribution from the VOC-limited regime. During 09:00 – 11:00, the fractions of the NO_x-limited and transitional regimes decrease, whereas the VOC-limited fraction increases. Taking 13:00 as a turning point, the former two regimes show an increase followed by a decrease, while the VOC-limited regime displays the opposite pattern. Compared with Beijing, the growth rate of the BLH in Nanjing is substantially weaker, whereas T_{2m} and RH are considerably higher. Such meteorological conditions may affect the efficiency of HO_2/RO_2 chain reactions, rendering ozone production more nonlinearly responsive to precursor changes and thereby leading to more complex dynamic behavior (Lu et al., 2019b). Consistent with this interpretation, the rates of change in $\Delta HCHO$ and ΔNO_2 (Fig. 9j) increase synchronously after 12:00, resulting in a transient rise in $\Delta HCHO/\Delta NO_2$; however, this elevated ratio is not sustained. This indicates that Nanjing does not stably enter a single-precursor-limited regime but instead remains largely within a transitional state characterized by joint VOC-NO_x control, reflecting strong photochemical activity under a NO_2 -rich background.

In contrast, Chengdu is dominated by a VOC-limited regime, followed by the transitional regime, while the NO_x-limited regime accounts for the smallest fraction. Before 12:00, the fractions of the NO_x-limited and transitional regimes decrease hourly, accompanied by a continuous increase in the VOC-limited fraction. After 12:00, although the VOC-limited fraction decreases slightly, it remains substantially higher than the other two regimes. Ozone formation in Chengdu is strongly influenced by basin-induced meteorological conditions: the enclosed topography restricts atmospheric dispersion and suppresses photochemical intensity, while sustained traffic and industrial emissions maintain relatively high NO_x levels, making ozone production more strongly constrained by VOC availability (Lu et al., 2019a). The rate-of-change characteristics of $\Delta HCHO$ and ΔNO_2 further support this interpretation. Compared with the other three cities, Chengdu exhibits the smallest variability in both $\Delta HCHO$ and ΔNO_2. During the morning (09:00 – 11:00), NO_2 continues to increase, whereas HCHO does not show a corresponding enhancement, limiting the amplification of radical chain reactions and thereby suppressing rapid ozone formation. Even in the afternoon, when NO_2 experiences sustained net loss and HCHO increases concurrently, $\Delta HCHO/\Delta NO_2$ remains persistently low, indicating that ozone

https://doi.org/10.5194/egusphere-2025-5424
Preprint. Discussion started: 27 January 2026

formation in Chengdu is consistently dominated by a VOC-limited regime.

In Guangzhou, ozone formation is dominated by the transitional regime before 12:00, followed by the NO_x-limited and VOC-limited regimes. After 12:00, the VOC-limited regime disappears, and ozone formation gradually shifts toward a pattern dominated by the NO_x-limited regime, with the transitional regime as secondary. Guangzhou exhibits the T_{2m} and RH among the four cities, reflecting a typical hot and humid coastal climate in southern China. Under emission conditions characterized by the coexistence of high NO_x levels and abundant reactive VOC_s, together with strong photochemical activity, NO_2 is rapidly photolyzed, while the continuously increasing emissions and oxidation of biogenic and anthropogenic VOC_s in the southern coastal region sustain high HCHO concentrations. This feature results in a persistently low fraction of the VOC-limited regime (Wang et al., 2021b; Wei et al., 2023). After 12:00, the net loss rate of NO_2 weakens rapidly, whereas HCHO maintains stable positive production, leading to a pronounced short-term enhancement in the marginal sensitivity of ozone formation to NO_x and a progressive transition toward a NO_x-limited regime. Overall, Guangzhou is characterized by an HCHO-abundant regime driven by strong biogenic and anthropogenic VOC emissions. These features are consistent with previous understandings of ozone formation mechanisms in eastern and southern Chinese cities (Wang et al., 2021a; Wang et al., 2025c).

Therefore, effective ozone pollution control should avoid single-precursor strategies and instead implement coordinated and time-dependent reductions of VOC_s and NO_x tailored to different regions and meteorological conditions to achieve stable and effective ozone mitigation.

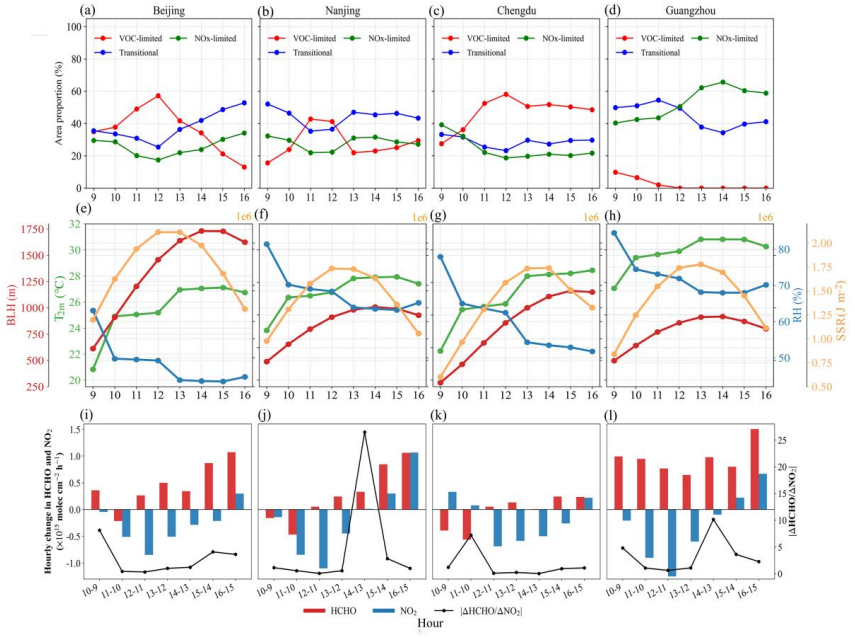

Figure 9. O_3 formation regimes and hourly variations in meteorological conditions and precursors for representative cities (Beijing(a,e,i), Nanjing(b,f,j), Chengdu(c,g,k), and Guangzhou(d,h,l)). **(a-d)** fractional contributions of O_3 formation regimes. **(e-h)** hourly time series of meteorological variables (BLH, T_{2m}, RH, SSR). **(i-l)** hourly rates of change in $\Delta HCHO$ and ΔNO_2.

4 Conclusions and Outlook

https://doi.org/10.5194/egusphere-2025-5424
Preprint. Discussion started: 27 January 2026

HCHO is a key intermediate in photochemical reactions involving VOC_s and serves as a precursor for ozone formation. Here, utilizing GEMS satellite technology and ground-based monitoring stations, we analyzed the relationship between meteorological factors and the spatiotemporal distribution of O_3-NO_x-VOC_s from 9:00 to 16:00 in major Chinese regions, based on daily O_3-NO_2-HCHO data and meteorological parameters from the warm seasons of 2021–2023. In addition, the sensitivity characteristics of the HCHO-to-NO_2 relationship were examined to analyze the spatiotemporal characteristics of O_3 formation and the differences in formation mechanisms across major regions of China and representative cities (Beijing, Nanjing, Chengdu, and Guangzhou). The main conclusions are summarized as follows:

O_3 and HCHO concentrations generally exhibited an upward trend from 09:00 to 16:00, peaking at 15:00 and 16:00, respectively. In contrast, NO_2 concentrations generally declined, with a notable rebound only at 10:00. Spatially, elevated levles of O_3, NO_2 and HCHO were concentrated in the BTH, YRD, SC and PRD regions. Meteoroloigcally, both T_{2m} and SSR exerted positive effects on ozone and HCHO concentrations. Meanwhile, enhanced photochemical activity and increased boundary layer height occasionally led to a reduction in nitrogen dioxide levels.

The scatter plot indicates that NO_x reaches saturation at 09:00. During the afternoon period (after 12:00), the ozone formation environment exhibits a distinct non-linear trend characterized by high VOC concentrations and low NO_2 concentrations. Moreover, compared to cubic polynomial fitting, LOESS fitting better highlights the diurnal variation characteristics of the quantitative relationship between FNR. Particularly after 12:00, the nonlinear relationship between O_3-NO_x-VOC_s exhibits $R^2 \geq 0.88$, The O_3 sensitivity curve remains consistent, peaking at 15:00 (1.97) with values ranging between [1.40–2.45].

From the spatio-temporal distribution of ozone formation mechanisms, China's primary regions remain predominantly NO_x-limited, with VOC-limited and transitional zones concentrated in the northern study area and parts of SC. Temporally, VOC-limited zones peak between 11:00 and 12:00, while transitional zones expand after 13:00. Additionally, the PRD region gradually transitioned from a VOC-limited pattern towards NO_x-limited and transitional modes between 2021 and 2023.

With respect to the dominant drivers of the diurnal variation in ozone formation sensitivity across major urban regions, Beijing, Nanjing, Chengdu, and Guangzhou are selected as representative cities for the BTH, YRD, SC and PRD regions, respectively. The results show that Beijing, under a NO_x-rich emission background, exhibits a VOC-limited regime driven by strong solar radiation and rapid boundary layer development, and transitions toward a transitional regime in the afternoon. Nanjing is dominated by a transitional regime jointly controlled by VOC_s and NO_x under hot and humid meteorological conditions, with complex diurnal variability arising from the nonlinear photochemical response of ozone formation to its precursors. Chengdu is dominated by a VOC-limited regime, primarily driven by basin-induced constraints on atmospheric dispersion that lead to persistent NO_x accumulation and relatively weak photochemical activity, resulting in a comparatively stable diurnal pattern. Guangzhou, under hot and humid climatic conditions, experiences persistently high HCHO levels driven by active biogenic and anthropogenic VOC emissions, which promote a transition of ozone formation toward a NO_x-limited regime.

It should be noted that this study still has some limitations in characterizing ozone formation mechanisms. On the one hand, the formation processes of ozone precursors within the study regions have not been explicitly examined, including anthropogenic sources (such as industrial, traffic, and power generation emissions) as well as other influencing factors such as atmospheric pressure,

https://doi.org/10.5194/egusphere-2025-5424
Preprint. Discussion started: 27 January 2026

precipitation, and vegetation, and a detailed source apportionment of ozone over major regions of China is lacking. On the other hand, the suppressive effects of aerosols on ozone formation—through the attenuation of solar radiation and the reduction of photolysis rates—are not considered, which may further influence the diagnosis of ozone sensitivity to NO_x and VOC_s. Future research will integrate regional air quality models, high-resolution anthropogenic VOC emission inventories, and aerosol-radiation interaction processes to systematically analyze the nonlinear response characteristics of O_3-VOC-NO_x, in order to support the formulation of precise emission reduction and coordinated control strategies for different periods and regions.

Data availability. GEMS satellite data (level-2 tropospheric NO_2 and HCHO data) are accessible via the National Institute of Environmental Research (NIER) website (https://nesc.nier.go.kr/ko/html/Index.do). Ground-based ozone station data originate from the China National Atmospheric Environment Monitoring Network (https://air.cnemc.cn:18007/). Land use type remote sensing data (30-metre resolution) can be found at https://www.resdc.cn/DOI/doi.aspx?DOIid=54. 2-meter temperature (T2m), relative humidity (RH), near-surface net radiation flux (SSR), and boundary layer height (BLH) can be downloaded from the ERA5 database (https://psl.noaa.gov/data/gridded/data.ncep.reanalysis.html).

Author contributions.Conceptualization: FQ and MM. Methodology: FQ. Investigation: CH, JW and YJ. Visualization: YJ and MM. Supervision: QF and JK. Writing—original draft: YJ, CH and MM. Writing—review & editing: MM. and JK.

Competing interests. The contact author has declared that none of the authors has any competing interests.

Acknowledgements. The GEMS team is gratefully acknowledged for their valuable data and technical support in this study.

Financial support. This work was supported by the Science and Technology Program of Guangdong Province (Science and Technology Innovation Platform Category) (Grant No. 2019B121201002), and the National Natural Science Foundation of China (Grant No. 42075181, 42375182, and 42175086).

References

Akimoto.: Global Air Quality and Pollution, Science., 302, 1716-1719, https://doi.org/10.1126/science.1092666, 2004.

Acdan, J. J., Pierce, R. B., Dickens, A. F., Adelman, Z., and Nergui, T.: Examining TROPOMI formaldehyde to nitrogen dioxide ratios in the Lake Michigan region: implications for ozone exceedances, Atmos. Chem. Phys., 23, 7867–7885, https://doi.org/10.5194/acp-23-7867-2023, 2023.

Bhartia, P.K.: OMI algorithm theoretical basis document, volume II, OMI ozone products, In NASA-OMI (Ed.), Washington, DC: ATBD-OMI-02, 2002.

Bin, C., Wang, Y. X., Huang, J. P., Zhao, L., Chen, R. M., Song, Z. H., and Hu, J. H.: Estimation of near-surface ozone concentration and analysis of main weather situation in Chin

https://doi.org/10.5194/egusphere-2025-5424
Preprint. Discussion started: 27 January 2026

a based on machine learning model and Himawari-8 TOAR data, The Science of the total environment, 864, 160928-160928, https://doi.org/10.1016/J.SCITOTENV.2022.160928, 2022.

Baek, K., Kim, J. H., Bak, J., Haffner, D. P., Kang, M., and Hong, H.: Evaluation of total oz one measurements from Geostationary Environmental Monitoring Spectrometer (GEMS), At mos. Meas. Tech., 16, 5461–5478, https://doi.org/10.5194/amt-16-5461-2023, 2023.

Chen, Y., Wang, M., Yao, Y., Zeng, C., Zhang, W., Yan, H., Gao, P., Fan, L., and Ye, D.: Res earch on the Ozone Formation Sensitivity Indicator of Four Urban Agglomerations of Chin a Using Ozone Monitoring Instrument (OMI) Satellite Data and Ground-Based Measureme nts, Sci. Total Environ., 869, 161679, https://doi.org/10.1016/J.SCITOTENV.2023.161679, 20 23.

Chen, J. J., Shen, H. F., Li, X. H., Li, T. W., and Wei, Y.: Ground-level ozone estimation bas ed on geo-intelligent machine learning by fusing in-situ observations, remote sensing data, and model simulation data, International Journal of Applied Earth Observation and Geoinfo rmation, 112, https://doi.org/10.1016/J.JAG.2022.102955. 2022.

Coates, J., Mar, K., Ojha, N., and Butler T.: The influence of temperature on ozone production under varying NO_x conditions – a modelling study, Atmos. Chem. Phys., 16, 11601–1161 5, https://doi.org/10.5194/acp-16-11601-2016, 2016.

Chang, C. Y., Faust, E., Hou, X. T., Lee, P. K., Hyun, C. K., Brent, C. H., and Liao, K. J.: I nvestigating ambient ozone formation regimes in neighboring cities of shale plays in the Northeast United States using photochemical modeling and satellite retrievals, Atmospheric Environment, 142, 152-170, https://link.cnki.net/doi/10.1016/j.atmosenv.2016.06.058, 2016.

Du, X. H., Tang, W., Zhang, Z. Z., Li, Y., Yu, Y., Xiao, Z. S., and Meng, F.: Sensitivity mod eling of ozone and its precursors over the Chengdu metropolitan area, Atmospheric Enviro nment, 277, https://doi.org/10.1016/J.ATMOSENV.2022.119071, 2022a.

Du, X. H., Wei, T., Cheng, M. M., Zhang, Z. Z., Li, Y., Li, Y., and Fan, M.: Modeling of sp atial and temporal variations of ozone-NO_x-VOC sensitivity based on photochemical indicat ors in China, Journal of Environmental Sciences, 114, 454-464, https://doi.org/10.1016/J.JES. 2021.12.026, 2022b.

Elise, P., and Tracey, H.: Evaluating current satellite capability to observe diurnal change in nit rogen oxides in preparation for geostationary satellite missions, Environmental Research Le tters, 15, 034038-034038, https://doi.org/10.1088/1748-9326/ab6b36, 2020.

Feng, Z. Z., Xu, Y. S., Kobayashi, K., Dai, L. L., Zhang, T. Y., Agathokleous, E., Calatayud, V., Paoletti, E., Mukherjee, A., Agrawal, M., Park, R. J., Oak, Y. J., and Yue, X.: Ozone pollution threatens the production of major staple crops in East Asia, Nature Food, 3, 47- 56, https://doi.org/10.1038/S43016-021-00422-6, 2022.

Feng, Z. H., Alessandra, D. M., Alessandro, A., Maurizio, G., Pierre, S., Tian, H. Q., Francesc a, F., Tao, F. L., Guo, A. H., and Elena, P.: Economic losses due to ozone impacts on hu man health, forest productivity and crop yield across China, Environment International, 131, 104966, https://doi.org/10.1016/j.envint.2019.104966, 2019.

Grytsai, A., and Milinevsky, G.: SCIAMACHY/Envisat, OMI/Aura, and ground-based total ozon e measurements over Kyiv-Goloseyev station, International Journal of Remote Sensing, 34, 5611-5622, https://doi.org/10.1080/01431161.2013.794988, 2013.

Georgiana, G., Sabina, Ş., Constantin, R., and Cristinel, G.: Assessing of surface-ozone concent

https://doi.org/10.5194/egusphere-2025-5424
Preprint. Discussion started: 27 January 2026

ration in Bucharest, Romania, using OML and satellite data, Atmospheric Pollution Research, 7, 567-576, https://doi.org/10.1016/j.apr.2016.02.001, 2016.

Han, T., Hu, X. M., Zhang, J., Xue, W. H., Che, Y. F., Deng, X. Q., and Zhou, L. H.: Rebuilding high-quality near-surface ozone data based on the combination of WRF-Chem model with a machine learning method to better estimate its impact on crop yields in the Beijing-Tianjin-Hebei region from 2014 to 2019, Environmental pollution, 336, 122334-122334, https://doi.org/10.1016/J.ENVPOL.2023.122334, 2023.

Itahashi, S., Yumimoto, K., Uno, I., Kurokawa, J., Ohara, T., Morino, Y., and Nagashima, T.: Fifteen-year trends (2005–2019) in the satellite-derived HCHO and NO_2 columns over East Asia, Remote Sensing, 14, 4512, https://doi.org/10.3390/rs14184512, 2022.

Jin, X., Fiore, A., Boersma, K. F., Smedt, I. D., and Valin, L.: Inferring Changes in Summertime Surface Ozone–NO_x–VOC Chemistry over U.S. Urban Areas from Two Decades of Satellite and Ground-Based Observations, Environ. Sci. Technol., 54, 6518–6529, https://doi.org/10.1021/acs.est.9b07785, 2020.

Jin, X. M., Arlene, M. F., Lee, T. M., Lukas, C. V., Lok, N. L., Bryan, D. K., Folkert, B., Isabelle, D. S., Gonzalo, G. A., Kelly, C., and Gail, S. T.: Evaluating a space-based indicator of surface ozone-NO_x-VOC sensitivity over midlatitude source regions and application to decadal trends, J. Geophys. Res. Atmos., 122, 10439–10461, https://doi.org/10.1002/2017JD026720, 2017.

Jing, F., Chao, Y., Li, Y. C., Ying, Z., Meng, F., Tao, J. H., and Chen, L. F.: Comparison of FNR and GNR Based on TROPOMI Satellite Data for Ozone Sensitivity Analysis in Chinese Urban Agglomerations, Remote Sensing, 17, 3321-332, https://doi.org/10.3390/RS17193321, 2025.

Javed, Z., Liu, C., Khokhar, M. F., Tan, W., Liu, H., Xing, C., Ji, X., Tanvir, A., Hong, Q., and Sandhu, O.: Ground-Based MAX-DOAS Observations of CHOCHO and HCHO in Beijing and Baoding, China, Remote Sens., 11, 1524, https://doi.org/10.5194/acpd-12-3983-2012, 2019.

Jin, X., and Holloway, T.: Spatial and temporal variability of ozone sensitivity over China observed from the Ozone Monitoring Instrument, Journal of Geophysical Research: Atmospheres, 120, 7229–7246, https://doi.org/10.1002/2015JD023250, 2015.

Kleinman, L. I., Daum, P. H., Lee, Y. N., Nunnermacker, L. J., Springston, S. R., Weinstein-Lloyd, J., and Rudolph, J.: A comparative study of ozone production in five U.S. metropolitan areas, Journal of Geophysical Research, 110, D02301, https://doi.org/10.1029/2004JD005096, 2005.

Klára, Č., Kamil, L., Ladislav, M., and Martin, S.: Intercomparison of Ground- and Satellite-Based Total Ozone Data Products at Marambio Base, Antarctic Peninsula Region, Atmosphere, 10, https://doi.org/10.3390/atmos10110721, 2019.

Kim, J., Jeong, U., Ahn, M. h., Kim, J. H., Park, R. J., Lee, H. L., Song, C. H., Choi, Y. S., Lee, K. H., Yoo, J. M., Jeong, M. J., Park, S. K., Lee, K. M., Song, C. K., Kim, S. W., Kim, Y. J., Kim, S. W., Kim, M. J., Go, S. J., Liu, X., Chance, K., Miller, C. C., Jay, A. S., Ben, V., Bhartia, P. K., Torres, O., Abad, G. G., Haffner, D. P., Ho, K. D., Lee, S. H., Woo, J. H., Chong, H. S., Park, S. S., Nicks, D., and Cho, W. J.: New era of air quality monitoring from space: Geostationary Environment Monitoring Spectrometer (GEMS), Bull. Am. Meteorol. Soc., 101, E1–E22, https://doi.org/10.1175/BAMS-D-18-0013.1, 2020.

https://doi.org/10.5194/egusphere-2025-5424
Preprint. Discussion started: 27 January 2026

Kim, S., and Kim, D.: First-time comparison between NO_2 vertical columns from Geostationary Environmental Monitoring Spectrometer (GEMS) and Pandora measurements, Atmos. Meas. Tech., 16, 3959–3972, https://doi.org/10.5194/amt-16-3959-2023, 2023.

Kelly, N. A., Wolff, G. T., and Ferman, M. A.: Sources and sinks of ozone in rural areas, At mos. Environ., 18, 1251–1266, https://doi.org/10.1016/0004-6981(84)90036-2, 1984.

Liang, Y. N., Wang, X. H., Qi, S. M., Xu, J. M., and Liu R.: Analysis of Ozone Formation S ensitivity in Guangdong Province Based on OMI Satellite and Ground Observation Data, E nvironmental Science, 45, 6248-6254, https://doi.org/10.13227/j.hjkx.202311261, 2024.

Liu, C. Q., and Shi, K.: A review on methodology in O_3-NO_x-VOC sensitivity study, Environm ental Pollution, 291, 118249-118249, https://doi.org/10.1016/J.ENVPOL.2021.118249, 2021.

Li, Z. K.: Nonlinear responses of ozone and its precursors and control strategies in the Pearl River, Ph.D. thesis, South China University of Technology, China, https://kns.cnki.net/kcms2/article/abstract?v=CeTIW1Ci4b03H3XltRrYGm3j24nM-2ZEag1rBEF0gz-DuXyagqymhLMSoswUwcREHljiL3_XwQICI_Z3gMhuM4_XbaFiYNeLuyPBKk3iwgaefYcRhnvdm1tD_lOglNmirZ5jjovCZ2U3mrqiC1fTPPicHFnPbu4SzR-ndxZQJBAtEmAb4IO92Zg0mfj4Htjp&uniplatform=NZKPT&language=CHS, 2023.

Li, Y.: Study on Ozone Formation Sensitivity in the Pearl River Delta Based on Satellite Rem ote Sensing and Air Quality Models, Ph.D. thesis, South China University of Technology, China, https://doi.org/10.27151/d.cnki.ghnlu.2021.005599, 2021.

Lyu, C. G., Zhang, W. M., Zhang, C., Shi, Y. F., Zhang, Y., and Wang, Y. P.: Evaluating the spatial representativeness of ground-based observations for satellite total ozone products, Int ernational Journal of Applied Earth Observation and Geoinformation, 129, 103778, https://doi.org/10.1016/J.JAG.2024.103778, 2024.

Li, T. W., and Chen, X.: Estimating daily full-coverage surface ozone concentration using satell ite observations and a spatiotemporally embedded deep learning approach, International Jou rnal of Applied Earth Observations and Geoinformation, 101, https://doi.org/10.1016/J.JAG.2021.102356, 2021.

Liu, Y. H., Zhou, H. H., Wei, W. Y., Chen, X. S., Zhou, M., Liu, Y. H., Ma, X. F., Yang, X. P., Song, H., Chen, X. R., Wang, H. C., Tan, Z. F., Wang, Z. F., Zhang, Y. H., and Lu, K. D.: Development and Evaluation of Mechanism for Air pollution complex version 1.0 (MAX1), Advances in Atmospheric Sciences, 43, 695-705, https://doi.org/10.1007/S00376-025-4456-Z, 2025.

Lee, G. T., Park, R. J., Kwon, H. A., Ha, E. S., Lee, S. D., Shin., Seunga, A. M., Kang, M., Choi, Y. S., and Kim, G.: First evaluation of the GEMS formaldehyde product against T ROPOMI and ground-based column measurements during the in-orbit test period, Atmos. Chem. Phys., 24, 4733–4749, https://doi.org/10.5194/egusphere-2023-1918, 2024.

Li, D. R., Wang, S. S., Xue, R. B., Zhu, J., Zhang, S. B., Sun, Z. B., and Zhou, B.: OMI-observed HCHO in Shanghai, China, during 2010–2019 and ozone sensitivity inferred by an improved HCHO/ NO_2 ratio, Atmospheric Chemistry and Physics, 21, 15447-15460, https://doi.org/10.5194/ACP-21-15447-2021, 2021.

Liu, Y., and Wang, T.: Worsening urban ozone pollution in China from 2013 to 2017 – Part 1: The complex and varying roles of meteorology, Atmos. Chem. Phys., 20, 6305–6321, https://doi.org/ 10.1073/pnas.1812168116, 2020.

Li, Y., Yu, C., Tao, J., Lu, X., and Chen, L.: Analysis of Ozone Formation Sensitivity in Chin

https://doi.org/10.5194/egusphere-2025-5424
Preprint. Discussion started: 27 January 2026

ese Representative Regions Using Satellite and Ground-Based Data, Remote Sens., 16, 316, https://doi.org/10.3390/RS16020316, 2024.

Lu, X., Zhang, L., and Shen, L.: Meteorology and Climate Influences on Tropospheric Ozone: a Review of Natural Sources, Chemistry, and Transport Patterns, Current Pollution Reports, 5, 238-260, https://doi.org/10.1007/s40726-019-00118-3, 2019b.

Lu, X., Zhang, L., Chen, Y. F., Zhou, M., Zheng, B., Li, K., Liu, Y. M., Lin, J. T., Fu, T. M., and Zhang, Q.: Exploring 2016–2017 surface ozone pollution over China: source contr ibutions and meteorological influences, Atmospheric Chemistry and Physics, 19, 8339-8361. https://doi.org/10.5194/acp-19-8339-2019, 2019a.

Maji, K. J., and Namdeo, A.: Continuous increases of surface ozone and associated premature mortality growth in China during 2015–2019, Environmental Pollution, 269, 116183, https:/ /doi.org/10.1016/J.ENVPOL.2020.116183, 2021.

Mahajan, A. S., Isabelle, D. S., Mriganka, S. B., Sachin, G., Suvarna, F., Chaitri, R., and Mic hel, V. R.: Inter-annual variations in satellite observations of nitrogen dioxide and formalde hyde over India, Atmospheric Environment, 116, 194-201, https://doi.org/10.1016/j.atmosenv. 2015.06.004, 2015.

Min, S., Wang, W. J., Bin, Y., David, D. P., Li, X., Lu, K. D., Wu, L. L., Wang, X. M., Mo, Z. W., Yang, S. X., Peng, Y, W., Kuang, Y., Chen, W. H., Hu, M., Zeng, L, M., Su, H., Cheng, Y. F., Zheng, J. Y., and Zhang, Y. H.: Quantifying the role of $PM_{2.5}$ dropping in variations of ground-level ozone: Inter-comparison between Beijing and Los Angeles, Scien ce of the Total Environment, 788, 147712, https://doi.org/10.1016/j.scitotenv.2021.147712, 2 021.

Oak, Y. J., Jacob, D. J., Balasus, N., Yang, L. H., Chong, H., Park, J., Lee, H., Lee, G. T., H a, E. S., Park, R. J., Kwon, H. A., and Kim, J.: A bias-corrected GEMS geostationary sa tellite product for nitrogen dioxide using machine learning to enforce consistency with the TROPOMI satellite instrument, Atmos. Meas. Tech., 17, 5147–5159, https://doi.org/10.5194 /amt-17-5147-2024, 2024.

Pan, Q. Q.: Spatiotemporal Distribution Characteristics of Ozone and Its Precursors in the Yang tze River Delta Region and Analysis of Ozone Formation Processes under Different NO_x E mission Scenarios, Ph.D. thesis, Donghua University, China, https://doi.org/10.27012/d.cnki.g dhuu.2023.001648, 2023.

Peng, H. C., Xing, C. Z., Li, Y. K., Zhang, C. X., Lin, J. N., Xue, J. K., Wang, X. H., Song, Y. H., Niu, X. H., and Liu, C.: Studies on regional ozone formation sensitivities and tran sport with higher spatiotemporal resolutions in a stereoscopic dimension: GEMS and vertic al observations, Atmospheric Research, 302, 107314, https://doi.org/10.1016/J.ATMOSRES.2 024.107314, 2024.

Paul, S. R., Kaitlin, C. D., Paul, J. W., Eric, E., Karsten, B., Philip, A. F., David, O. M., Will iam, H. B., Abigail, R. K., Joost, A. G., Pawel, K. M., Allen, H. G., and Ronald, C. C.: Effects of temperature-dependent NO_x emissions on continental ozone production, Atmosph eric Chemistry and Physics, 18, 2601-2614, https://doi.org/10.5194/acp-18-2601-2018, 2018.

Ren, J., Guo, F. F., and Xie, S. D.: Diagnosing ozone–NO_x–VOC sensitivity and revealing cau ses of ozone increases in China based on 2013–2021 satellite retrievals, Atmospheric Che mistry and Physics, 22, 15035-15047, https://doi.org/10.5194/ACP-22-15035-2022, 2022.

Sillman, S.: The use of NOy, H_2O_2, and HNO_3 as indicators for ozone–NO_x–hydrocarbon sensit

https://doi.org/10.5194/egusphere-2025-5424
Preprint. Discussion started: 27 January 2026

ivity 100, 14175–14188, Journal of Geophysical Research Atmospheres, https://doi.org/10.1029/94JD02953, 1995.

Sillman, S., and He, D.: Some theoretical results concerning O_3-NO-VOC chemistry and NO-VOC indicators, Geophys. Res. Atmos., 107, 1-15, https://doi.org/10.1029/2001JD001123, 2002.

Souri, A., Nowlan, C., Wolfe, G., Lamsal, L., Miller, C., Abad, G. G., Janz, S., Fried, A., Blake, D., Weinheimer, A., Diskin, G., Liu, X., and Chance, K.: Revisiting the effectiveness of HCHO/NO_2 ratios for inferring ozone sensitivity to its precursors using high resolution airborne remote sensing observations in a high ozone episode during the KORUS-AQ campaign, Atmos. Environ., 224, 117341, https://doi.org/10.1016/j.atmosenv.2020, 2020.

Sun, Y. W., Yin, H., Liu, C., Zhang, L., Cheng, Y., Palm, M., Notholt, J., Lu, X., Vigouroux, C., Zheng, B., Wang, W., Jones, N., Shan, C. G., Qin, M., Tian, Y., Hu, Q. H., Meng, F. H., and Liu, J. G.: Mapping the drivers of formaldehyde (HCHO) variability from 2015 to 2019 over eastern China: insights from Fourier transform infrared observation and GEOS-Chem model simulation, Atmospheric Chemistry and Physics, 21, 6365-6387, https://doi.org/10.5194/ACP-21-6365-2021, 2021.

Tan, Z., Lu, K., Jiang, M., Su, R., Wang, H., Lou, S., Fu, Q., Zhai, C., Tan, Q., and Yue, D.: Daytime atmospheric oxidation capacity in four Chinese megacities during the photochemically polluted season: a case study based on box model simulation, Atmos. Chem. Phys., 19, 3493–3513, https://doi.org/10.5194/acp-19-3493-2019, 2019.

Wang, M., Sheng, H., Liu, Y., Wang, G., Huang, H., Fan, L., and Ye, D.: Research on the Diurnal Variation Characteristics of Ozone Formation Sensitivity and the Impact of Ozone Pollution Control Measures in “2 + 26” Cities of Henan Province in Summer, Sci. Total Environ., 888, 164121, https://doi.org/10.1016/J.SCITOTENV.2023.164121, 2023.

Wu, W. L., Xue, W. B., Lei, Y., and Wang, J. N.: Sensitivity of Ozone Formation in the Beijing-Tianjin-Hebei Region and Surrounding Areas Based on OMI Data, China Environmental Science, 38, 1201-1208, https://doi.org/10.19674/j.cnki.issn1000-6923.2018.0143, 2018.

Wang, W. H., Liu, X., Bi, J. Z., and Liu, Y.: A machine learning model to estimate ground-level ozone concentrations in California using TROPOMI data and high-resolution meteorology, Environment International, 158, 106917-106917, https://doi.org/10.1016/J.ENVINT.2021.106917, 2022.

Wang, X. H., Shen, X. E., Jiang, L., Zhang, J., Sun, S., Li, L., and Song, X. K.: Analysis of changes in ozone precursors and formation sensitivity in the Beijing-Tianjin-Hebei region based on TROPOMI and Ground observations, China Environmental Science, 45, 6571-6583, https://doi.org/10.19674/j.cnki.issn1000-6923.20250721.003, 2025b.

Wang, R. F., Ma, X. D., Zhao, T. L., Wang, H. L., Ding, H., and Zheng, X. B.: Evaluation of the Applicability of MACC Reanalysis Ozone Data over China Using Ground-Based Observations and AIRS Satellite Data, Environmental Science, 40, 4412-4422, https://doi.org/10.13227/j.hjkx.201904029, 2019.

Wu, Y., Huo, J., Yang, G., Wang, Y., Wang, L., Wu, S., Yao, L., Fu, Q., and Wang, L.: Measurement report: Production and loss of atmospheric formaldehyde at a suburban site of Shanghai in summertime, Atmos. Chem. Phys., 23, 2997–3014, https://doi.org/10.5194/acp-2022-682, 2023.

Wang, W., Li, X., Cheng, Y., Parrish, D. D., Ni, R., Tan, Z., Liu, Y., Lu, S., Wu, Y., and Ch

https://doi.org/10.5194/egusphere-2025-5424
Preprint. Discussion started: 27 January 2026

757 en, S.: Ozone pollution mitigation strategy informed by long-term trends of atmospheric o
758 xidation capacity, Nat. Geosci., 17, 20–25, https://doi.org/10.1038/s41561-023-01334-9, 202
759 4.
760 Wang, Y. H., Lucas, A. J. B., Wang, Y. A., Jin, L., and Robert, A. H.: Temperature and stagn
761 ation effects on ozone sensitivity to NO_x and VOC: an adjoint modeling study in central
762 California, Atmospheric Chemistry and Physics, 25, 17651–17688, https://doi.org/10.5194/ac
763 p-25-17651-2025, 2025a.
764 Wang, J., Zhang, Y. L., Xiao, S. X., Wu, Z. F., and Wang, X. M.: Ozone Formation at a Sub
765 urban Site in the Pearl River Delta Region, China: Role of Biogenic Volatile Organic Co
766 mpounds, Atmosphere, 14, 609, https://doi.org/10.3390/atmos14040609, 2021b.
767 Wei, C. B., Yu, G. H., Cao, L. M., Han, H. X., Xia, S. Y., and Huang, X. F.: Tempo-spacial
768 variation and source apportionment of atmospheric formaldehyde in the Pearl River Delta,
769 China, Atmospheric Environment, 312, https://doi.org/10.1016/J.ATMOSENV.2023.120016, 2
770 023.
771 Wang, W., Van, D. A. R., Ding, J., Van, W. M., and Cheng, T.: Spatial and temporal changes
772 of the ozone sensitivity in China based on satellite and ground-based observations, Atmosp
773 heric Chemistry and Physics, 21, 7253–7272, https://doi.org/10.5194/acp-21-7253-2021, 2021
774 a.
775 Wang, Z., Zhang, H., Shi, C. E., Ji, X. G., Zhu, Y. Z., Xia, C. Z., Sun, X. Y., Zhang, M., Lin,
776 X. F., Yan, S. W., Zhou, Y., Xing, C. Z., Chen, Y. J., and Liu, C.: Vertical and spatial dif
777 ferences in ozone formation sensitivities under different ozone pollution levels in eastern C
778 hinese cities, npj Climate and Atmospheric Science, 8, 30-30, https://doi.org/10.1038/S4161
779 2-024-00855-3, 2025c.
780 Xu, W., Yang, H., He, M., Yang, Z., Zhang, Y., Liu, Z. h., and He, Y. M.: Spatiotemporal Dis
781 tribution and Influencing Factors of Ozone Formation Sensitivity in the Chengdu-Chongqin
782 g Region, Environmental Science, 46, 736-745, https://doi.org/10.13227/j.hjkx.202312065, 20
783 25.
784 Xu. J., Zhang. Z., Rao. L. L., Wang, Y. P., Yan, H. H., Hu, S. T., Shi, C., Liu, S., Gegen, T.,
785 Wang, W. Y., Shi, E., Yao, S., Zhu, J., Wang, Y. M., Dong, X. L., and Shi, J. C.: Tropo
786 spheric ozone retrieval from satellite remote sensing—a review, Advances in Earth Science,
787 39, 56-70, https://doi.org/10.11867/j.issn.1001-8166.2024.002, 2024.
788 Xie, M., Zhu, K., Wang, T., Chen, P., Han, Y., Li, S., Zhuang, B., and Shu, L.: Temporal cha
789 racterization and regional contribution to O_3 and NO_x at an urban and a suburban site in
790 Nanjing, China, Sci. Total Environ., 551–552, https://doi.org/10.1016/j.scitotenv.2016.02.047,
791 2016.
792 Xia, N., Du, E. Z., Guo, Z. D., and Wim, D. V.: The diurnal cycle of summer tropospheric o
793 zone concentrations across Chinese cities: Spatial patterns and main drivers, Environmental
794 Pollution, 286, 117547-117547, https://doi.org/10.1016/J.ENVPOL.2021.117547, 2021.
795 Yang, K. P., Liu, H. R., Xing, C. Z., Su, W. J., Hong, Q. Q., Li, Q. H., Ji, X. G., and Liu,
796 C.: Study on Tropospheric Ozone Characteristics in the Pearl River Delta Region Based o
797 n TROPOMI Observations, Journal of Atmospheric and Environmental Optics, 20, 47-59,
798 https://kns.cnki.net/kcms2/article/abstract?v=IC7xd21WxIgGWOCGHFjrWcJdWGGUXTUtn1
799 MdXPLthyYjTgTKSephpq9a9Ps9sajJR9fgJE81QBSu6JRWKnNSQYWRNnRiDHOHFSkq_Ddtf
800 VzeBFsRGluXg5OwAyP3QAD1Kmf9L6E8Sdh4z2tYojS2PUsNg7DPCMwAgJFBMBFZKeekT_

https://doi.org/10.5194/egusphere-2025-5424
Preprint. Discussion started: 27 January 2026

g0k2fUow==&uniplatform=NZKPT&language=CHS, 2025.

Yu, L., Cheng, M. M., Guo, Z., Zhang, X. Y., Cui, X. M., and Chen, S. G.: Increase in Surface Ozone over Beijing-Tianjin-Hebei and the Surrounding Areas of China Inferred from Satellite Retrievals, 2005-2018, Aerosol and Air Quality Research, 20, 2170-2184, https://doi.org/10.4209/aaqr.2019.11.0603, 2020.

Yang, W., Lampel, J., Xie, P., Beirle, S., and Wagner, T.: Ground-based MAX-DOAS observations of tropospheric aerosols, NO_2, SO_2 and HCHO in Wuxi, China, from 2011 to 2014, Atmos. Chem. Phys., 17, 2189–2215, https://doi.org/10.5194/acp-17-2189-2017, 2017.

Yang, Y. M, Li, X., Zu, K. X., Lian, C. F., Chen, S. Y., Dong, H. B., Feng, M., Liu, H. F., Liu, J. W., Lu, K. D., Lu, S. H., Ma, X. F., Song, D. L., Wang, W. G., Yang, S. D., Yang, X. P., Yu, X. N., Zhu, Y., Zeng, L. M., Tan, Q. W., and Zhang, Y. H.: Elucidating the effect of HONO on O_3 pollution by a case study in southwest China, Science of the Total Environment, 756, https://doi.org/10.1016/J.SCITOTENV.2020.144127, 2021.

Yang, X., Wu, K., Wang, H., Liu, Y., and Wang, Z.: Summertime ozone pollution in Sichuan Basin, China: Meteorological conditions, sources and process analysis, Atmos. Environ., 226, 117392, https://doi.org/10.1016/j.atmosenv.2020.117392, 2020.

Zhou, H., Wang, M., Chai, W. X., and Zhao, X.: Analysis of Ozone Sensitivity in Beijing Urban Area Based on Random Forest, Environmental Science, 45, 2497-2506, https://doi.org/10.13227/j.hjkx.202306034, 2024.

Zhang, Y. Z., Wang, Y. H., Crawford, J., Cheng, Y., and Li, J. F.: Improve observation-based ground-level ozone spatial distribution by compositing satellite and surface observations: A simulation experiment, Atmospheric Environment, 180, 226-233, https://doi.org/10.1016/j.atmosenv.2018.02.044, 2018.

Zhang, X. Y., Zhao, L. M., Cheng, M. M., and Chen, D. M.: Estimating Ground-Level Ozone Concentrations in Eastern China Using Satellite-Based Precursors, IEEE Transactions on Geoscience and Remote Sensing, 1-10, https://doi.org/10.1109/tgrs.2020.2966780, 2020.

Zhang, K., and Batterman, S. A.: Time allocation shifts and pollutant exposure due to traffic congestion: an analysis using the national human activity pattern survey, Sci. total environ., 407, 5493–5500, https://doi.org/10.1016/j.scitotenv.2009.07.008, 2009.

Zhang, J. X., Gao, Y., Leung, L. R., Luo, K., Wang, M. H., Zhang, Y., Bell, M. L., and Fan, J. R.: Disentangling the mechanism of temperature and water vapor modulation on ozone under a warming climate, Environmental Research Letters, 17, https://doi.org/10.1088/1748-9326/ACA3BC, 2022.